# 10

# Power Quality Enhancement using Predictive Controlled Multilevel Converters

João Dionísio Simões Barros[1] and José Fernando Alves da Silva[2]
[1]*University of Madeira,*
[2]*Instituto Superior Técnico, Technical University of Lisbon*
*Portugal*

## 1. Introduction

Electrical power is one of the factors that most influences the economic development of our society. Since the beginning of the use of electricity the continuous improvement of generation, distribution and use of electricity tries to satisfy the ever increasing quality and performance needs of most sectors of human activity.

The power quality of the electrical network is mainly related to the technical characteristics of the voltage waveform at a given point of the electrical power network. The quality of the AC voltage can be evaluated, considering that electrical power networks should provide constant frequency constant amplitude pure sinusoidal voltages, with 120° phase shift between phases. Voltage deviations from these characteristics of the sinusoidal waveforms, imply a loss of power quality (Moreno-Muñoz, 2007), (Tan et al., 2005).

To mitigate some power quality issues, dynamic adjustable solutions based on electronic power converters have been developed. These power converters must use fully controlled (turn-on and turn-off) power semiconductor switching devices to reduce the harmonic content of currents in the electrical power network. These converters can perform as active power filters (APF) (Singh et al., 1999), to cancel disturbing current or voltage harmonics, or Unity Power Factor Rectifiers (UPFR) to obtain almost sinusoidal and in phase AC currents.

The dynamic voltage restorer (DVR) is an advantageous solution to mitigate power quality problems such as sags, ripple, flicker, transients or swells, and to reduce the susceptibility of loads (or people) sensitive to them.

This chapter presents the optimal predictive control of power converters applied to power quality enhancement procedures. A three-level, three-phase neutral point clamped multilevel (NPC) converter, useful in medium voltage applications, is considered. The predictive optimal controllers and fundamental frequency synchronizers are designed, and applied to control the NPC converter AC currents and to balance the DC capacitor voltages in applications such as:

1. Active Power Filters (APF)
2. Unity Power Factor Rectifiers (UPFR)
3. High Quality Dynamic Voltage Restorers (DVR)

Simulation and experimental results show that the AC currents and voltages are almost sinusoidal (THD less than 1%) in steady state operation, but also when facing balanced and

unbalanced sags, distorted network voltages and short interruptions with unbalanced loads, or high level of non-linear distorted currents.

## 2. Optimal predictive control for power converters

Multilevel converters are designed to inherently share their usually DC high voltage power supply evenly between cascaded power semiconductors. Therefore, they are suitable for high voltage, high power applications despite DC voltage balancing problems and complex modulation, compared to two-level converters (Holmes & Lipo, 2003).
There are some available multilevel converter topologies, being the Neutral Point Clamped (NPC) (Nabae & Takahashi, 1981), Flying Capacitor (Meynard & Foch, 1992), and Cascaded H-bridge (Marchesoni et al., 1988) the most reported in literature (Holmes & Lipo, 2003).
Pulse-width modulation (PWM) and space vector modulation (SVM) are the most common control techniques used in multilevel power converters (Holmes & Lipo, 2003), even though the controlled outputs are often affected by power semiconductor switching times. Correctly designed control methods for multilevel converters based on hysteresis comparators, or sliding mode approaches, are robust to component mismatches, semiconductor switching times, present zero steady-state error, but need variable switching frequency, and DC voltages both usually higher than SVM and PWM to obtain better performance (Kazmierkowski & Malesani, 1998).
Optimal predictive controllers are based on the linear optimal control systems theory. Their aim is to solve the minimization problem of a cost functional. Therefore, predictive controllers can be tailored to minimize system output errors, DC voltage, and/or the switching frequency, at a given sampling frequency, being suitable to simultaneously control currents and voltages with non-linear and coupled dynamics (Kwakernaak, & Sivan, 1972).

### 2.1 Dynamic modeling of NPC multilevel converters

The dynamic models of the NPC multilevel converters are here derived and used to design the AC currents and DC voltages optimal predictive controllers. From the three-phase NPC 27 output voltage vectors are available. The optimal predictive controllers choose the best output voltage vector that minimizes the AC line alfa-beta (αβ) current errors, the total DC voltage regulation error and the unbalancing of partial DC capacitor voltages, $U_{C1}$ and $U_{C2}$.
The DC side of a Neutral-Point-Clamped multilevel converter (Fig. 1) includes a DC source $U_{dc}$ and DC voltage dividing capacitors $C_1$ and $C_2$. The switching variables $\gamma_k$ represent the state of the multilevel converter active switches, $S_{kj}$, with $k \in \{1, 2, 3\}$ and $j \in \{1, 2, 3, 4\}$. Assuming ideal semiconductors, the three combinations of the binary states of the switches $S_{kj}$ of each leg $k$ can be defined as:

$$\gamma_k = \begin{cases} 1 & \left(S_{k1} = 1 \wedge S_{k2} = 1\right) \wedge \left(S_{k3} = 0 \wedge S_{k4} = 0\right) \\ 0 & \left(S_{k1} = 0 \wedge S_{k2} = 1\right) \wedge \left(S_{k3} = 1 \wedge S_{k4} = 0\right) \\ -1 & \left(S_{k1} = 0 \wedge S_{k2} = 0\right) \wedge \left(S_{k3} = 1 \wedge S_{k4} = 1\right) \end{cases}. \tag{1}$$

Assuming that the optimum predictive controller balances the capacitor voltages $U_{C1}$ and $U_{C2}$, so that $U_{C1} \approx U_{C2} \approx U_{dc}/2$, the voltage $u_{mk}$ from each leg to the neutral point of the multilevel converter is:

$$u_{mk} = \gamma_k \frac{U_{dc}}{2}. \tag{2}$$

The NPC converter AC side is connected to the electrical power network voltages $U_{L1}$, $U_{L2}$, $U_{L3}$ trought three-phase inductors, $L$, with losses represented by resistor, $R$.

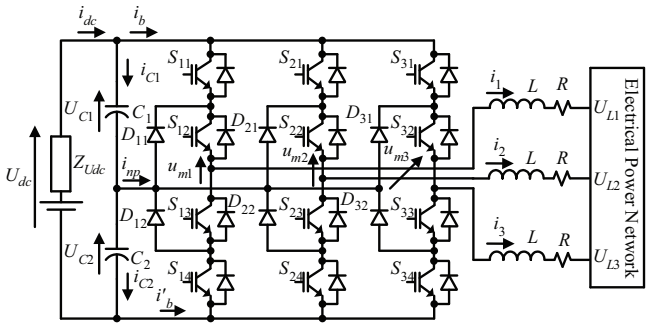


Fig. 1. Neutral-point-clamped multilevel converter circuit

### 2.1.1 Switched state-space multilevel converter model

Applying Kirchhoff laws to the NPC converter circuit (Fig. 1) and doing some algebraic manipulations, the dynamic equations of the AC currents, $i_1$, $i_2$, and $i_3$, and the capacitor voltages, $U_{C1}$ and $U_{C2}$, are obtained as functions of the circuit parameters and switching variables (3),

$$\begin{bmatrix} \frac{di_1}{dt} \\ \frac{di_2}{dt} \\ \frac{di_3}{dt} \\ \frac{dU_{C1}}{dt} \\ \frac{dU_{C2}}{dt} \end{bmatrix} = \begin{bmatrix} -\frac{R}{L} & 0 & 0 & \frac{\Xi_{11}}{L} & \frac{\Xi_{12}}{L} \\ 0 & -\frac{R}{L} & 0 & \frac{\Xi_{21}}{L} & \frac{\Xi_{22}}{L} \\ 0 & 0 & -\frac{R}{L} & \frac{\Xi_{31}}{L} & \frac{\Xi_{32}}{L} \\ -\frac{\Gamma_{11}}{C_1} & -\frac{\Gamma_{12}}{C_1} & -\frac{\Gamma_{13}}{C_1} & 0 & 0 \\ -\frac{\Gamma_{21}}{C_2} & -\frac{\Gamma_{22}}{C_2} & -\frac{\Gamma_{23}}{C_2} & 0 & 0 \end{bmatrix} \begin{bmatrix} i_1 \\ i_2 \\ i_3 \\ U_{C1} \\ U_{C2} \end{bmatrix} + \begin{bmatrix} -\frac{1}{L} & 0 & 0 & 0 \\ 0 & -\frac{1}{L} & 0 & 0 \\ 0 & 0 & -\frac{1}{L} & 0 \\ 0 & 0 & 0 & \frac{1}{C_1} \\ 0 & 0 & 0 & \frac{1}{C_2} \end{bmatrix} \begin{bmatrix} U_{L1} \\ U_{L2} \\ U_{L3} \\ i_{dc} \end{bmatrix} \tag{3}$$

where

$$\Gamma_{1k} = \frac{\gamma_k(\gamma_k+1)}{2};\ \Gamma_{2k} = \frac{\gamma_k(1-\gamma_k)}{2};\ \Xi_{ki} = \frac{1}{3}\left[2\Gamma_{ik} - \sum_{\substack{j=1 \\ j\neq k}}^{3}\Gamma_{ij}\right]. \tag{4}$$

For AC networks with isolated neutral (zero homopolar current), these equations can be simplified using αβ coordinates.

### 2.1.2 Switched state-space multilevel system model in αβ coordinates

The relationship between the variables $\mathbf{X_{123}}$ represented in system coordinates and in αβ coordinates (Jones, 1967), $\mathbf{X_{\alpha\beta}}$, is (**C** is the Clarke-Concordia transformation matrix)

$$\mathbf{X_{123}} = \mathbf{C}\mathbf{X_{\alpha\beta 0}}\ ;\ \mathbf{C} = \sqrt{\frac{2}{3}}\begin{bmatrix} 1 & 0 & \frac{\sqrt{2}}{2} \\ -\frac{1}{2} & \frac{\sqrt{3}}{2} & \frac{\sqrt{2}}{2} \\ -\frac{1}{2} & -\frac{\sqrt{3}}{2} & \frac{\sqrt{2}}{2} \end{bmatrix}. \tag{5}$$

Applying (5) to the model (3), and assuming zero homopolar current the multilevel model (6) in αβ coordinates is derived.

$$\begin{bmatrix} \frac{di_\alpha}{dt} \\ \frac{di_\beta}{dt} \\ \frac{dU_{C1}}{dt} \\ \frac{dU_{C2}}{dt} \end{bmatrix} = \begin{bmatrix} -\frac{R}{L} & 0 & \frac{\Gamma_{1\alpha}}{L} & \frac{\Gamma_{2\alpha}}{L} \\ 0 & -\frac{R}{L} & \frac{\Gamma_{1\beta}}{L} & \frac{\Gamma_{2\beta}}{L} \\ -\frac{\Gamma_{1\alpha}}{C_1} & -\frac{\Gamma_{1\beta}}{C_1} & 0 & 0 \\ -\frac{\Gamma_{2\alpha}}{C_2} & -\frac{\Gamma_{2\beta}}{C_2} & 0 & 0 \end{bmatrix} \begin{bmatrix} i_\alpha \\ i_\beta \\ U_{C1} \\ U_{C2} \end{bmatrix} + \begin{bmatrix} -\frac{1}{L} & 0 & 0 \\ 0 & -\frac{1}{L} & 0 \\ 0 & 0 & \frac{1}{C_1} \\ 0 & 0 & \frac{1}{C_2} \end{bmatrix} \begin{bmatrix} U_{L\alpha} \\ U_{L\beta} \\ i_{dc} \end{bmatrix} \tag{6}$$

Where

$$\Gamma_{i\alpha} = \sqrt{\frac{2}{3}}\left(\Gamma_{i1} - \frac{\Gamma_{i2}}{2} - \frac{\Gamma_{i3}}{2}\right);\ \Gamma_{i\beta} = \sqrt{\frac{2}{3}}\left(\frac{\sqrt{3}}{2}\Gamma_{i2} - \frac{\sqrt{3}}{2}\Gamma_{i3}\right). \tag{7}$$

This model is suitable to design the optimal predictive current controller, and the 27 possible combinations of $\Gamma_{i\alpha}$ and $\Gamma_{i\beta}$ values can be used to plot the 27 vectors of Fig. 2. (Values of $\gamma_1$, $\gamma_2$, and $\gamma_3$ are inside brackets).

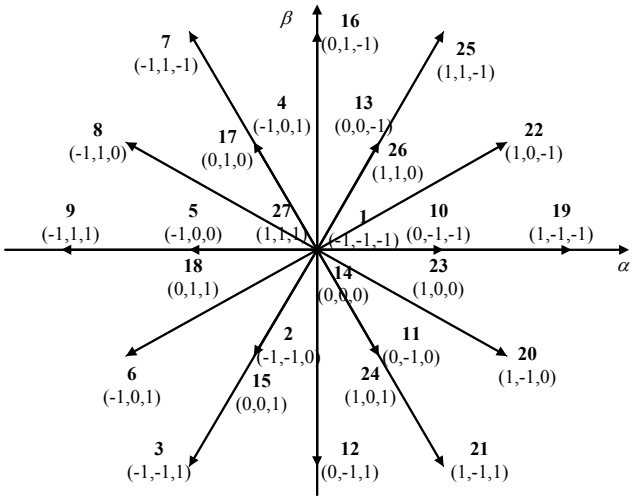


Fig. 2. Available voltage vectors at the output of the multilevel converter

### 2.1.3 Switched state-space multilevel system model in dq coordinates

Variables $\mathbf{X_{\alpha\beta}}$ in αβ coordinates are expressed in dq coordinates, $\mathbf{X_{dq}}$, using the Park transformation (Jones, 1967):

$$\mathbf{X_{\alpha\beta}} = \mathbf{D}\mathbf{X_{dq}}\,;\,\mathbf{D} = \begin{bmatrix} \cos\theta & -\sin\theta \\ \sin\theta & \cos\theta \end{bmatrix}. \tag{8}$$

The argument $\theta=\omega t+\theta_i$ is the angular phase of the electrical network AC line voltage with angular frequency $\omega$ and initial phase $\theta_i$. Applying the Park transformation (8) to (6), the NPC converter model (9) in dq coordinates is obtained.

$$\begin{bmatrix} \frac{di_d}{dt} \\ \frac{di_q}{dt} \\ \frac{dU_{C1}}{dt} \\ \frac{dU_{C2}}{dt} \end{bmatrix} = \begin{bmatrix} -\frac{R}{L} & \omega & \frac{\Gamma_{1d}}{L} & \frac{\Gamma_{2d}}{L} \\ -\omega & -\frac{R}{L} & \frac{\Gamma_{1q}}{L} & \frac{\Gamma_{2q}}{L} \\ -\frac{\Gamma_{1d}}{C_1} & -\frac{\Gamma_{1q}}{C_1} & 0 & 0 \\ -\frac{\Gamma_{2d}}{C_2} & -\frac{\Gamma_{2q}}{C_2} & 0 & 0 \end{bmatrix} \begin{bmatrix} i_d \\ i_q \\ U_{C1} \\ U_{C2} \end{bmatrix} + \begin{bmatrix} -\frac{1}{L} & 0 & 0 \\ 0 & -\frac{1}{L} & 0 \\ 0 & 0 & \frac{1}{C_1} \\ 0 & 0 & \frac{1}{C_2} \end{bmatrix} \begin{bmatrix} U_{Ld} \\ U_{Lq} \\ i_{dc} \end{bmatrix} \tag{9}$$

Where

$$\begin{bmatrix} \Gamma_{id} \\ \Gamma_{iq} \end{bmatrix} = \begin{bmatrix} \cos\theta & \sin\theta \\ -\sin\theta & \cos\theta \end{bmatrix} \begin{bmatrix} \Gamma_{i\alpha} \\ \Gamma_{i\beta} \end{bmatrix}; \text{ with } i \in \{1, 2\}. \tag{10}$$

This quasi-linear model of the state space variables is suitable to design non-optimum but simple linear controllers to control the multilevel converter.

### 2.2 Optimal predictive controller design

The obtained αβ NPC multilevel converter dynamic model (6) must be solved to estimate (predict) the state variables values at the next sampling period, for all the 27 available vectors of the NPC converter.

Using the predicted values and sampling the AC output currents and DC capacitor voltages, control errors are calculated for the next sampling time, using linearized models and considering the application of every one of the 27 output voltage vectors. Then, a suitable quadratic weighed cost functional is defined and evaluated to choose the voltage vector that minimizes the AC current tracking errors, the DC voltage steady-state error and the input DC capacitor voltage unbalancing.

### 2.2.1 Predictive equations for AC currents and DC capacitor voltages

From the decoupled model (6) the solution of the AC currents, $i_x$, with $x \in \{\alpha,\beta\}$, are found to be (Kwakernaak & Sivan, 1972)

$$i_x(t_{s+1}) \approx i_x(t_s) - \frac{R}{L}\Delta T i_x(t_s) + \frac{\Gamma_{1x}}{L}\Delta T U_{C1}(t_s) + \frac{\Gamma_{2x}}{L}\Delta T U_{C2}(t_s) - \frac{\Delta T}{L}U_{Lx}(t_s). \tag{11}$$

Where $i_x(t_s)$ are the currents $i_x(t)$ at the sampling instant $t_s = k\Delta T$ and $i_x(t_{s+1}) = i_x(t = (k+1)\ \Delta T)$ are the currents to be predicted for the next $(k+1)$ sampling interval $\Delta T$. Assuming a sampling time $\Delta T$ small enough, $U_{C1}(t_s)$, $U_{C2}(t_s)$, and $U_{Lx}(t_s)$ can all be considered nearly constant during $\Delta T$ (or its change can be further estimated). In order to predict the capacitor voltage difference, $U_{C1}(t)$-$U_{C2}(t)$, from the dynamic equations (6), the solution of the capacitor voltages are (Kwakernaak & Sivan, 1972)

$$U_{Ci}(t_{s+1}) \approx U_{Ci}(t_s) - \frac{\Gamma_{i\alpha}}{C_i}\Delta T i_\alpha(t_s) - \frac{\Gamma_{i\beta}}{C_i}\Delta T i_\beta(t_s) + \frac{\Delta T}{C_i} i_{dc}(t_s)\ ; \text{with } i \in \{1, 2\}. \tag{12}$$

Where $U_{Ci}(t_s)$ are the sampled capacitor voltages at $t = t_s = k\Delta T$. Considering $C_1 \approx C_2 \approx C$ and $\Delta T$ small enough so that the DC current, $i_{dc}(t)$, is nearly constant and assuming that the AC line currents follow their references, the capacitors voltage error is:

$$U_{C1}(t_{s+1}) - U_{C2}(t_{s+1}) \approx U_{C1}(t_s) - U_{C2}(t_s) + (\Gamma_{2\alpha} - \Gamma_{1\alpha})\frac{\Delta T}{C} i_\alpha(t_s) + (\Gamma_{2\beta} - \Gamma_{1\beta})\frac{\Delta T}{C} i_{L\beta}(t_s)\ . \tag{13}$$

### 2.2.2 Quadratic cost functional definition

A three-phase NPC converter operated as a current source has three variables to control, $i_\alpha(t)$, $i_\beta(t)$, and $U_{C1}(t)$-$U_{C2}(t)$ to ensure $U_{C1} \approx U_{C2} \approx U_{dc}/2$. The main objective of the optimizing controller is the minimization of both the AC currents errors and the capacitor voltage difference. Therefore, the quadratic cost functional contains weighted current errors and DC voltage difference (14).

$$C(t_{s+1}) = \sqrt{\frac{e_\alpha^2(t_{s+1})}{\rho_\alpha} + \frac{e_\beta^2(t_{s+1})}{\rho_\beta} + \frac{e_{UC}^2(t_{s+1})}{\rho_{UC}}} \tag{14}$$

Where

$$\begin{aligned} e_\alpha(t_{s+1}) &= i_{\alpha \mathrm{Re}f}(t_{s+1}) - i_\alpha(t_{s+1}); \\ e_\beta(t_{s+1}) &= i_{\beta \mathrm{Re}f}(t_{s+1}) - i_\beta(t_{s+1}); \\ e_{UC}(t_{s+1}) &= U_{C1}(t_{s+1}) - U_{C2}(t_{s+1}). \end{aligned} \tag{15}$$

In the cost functional (14) the errors are weighted with the weights $\rho_\alpha$, $\rho_\beta$, and $\rho_{UC}$. The weights have two purposes: they normalize the distinct errors, which have different units and ranges, with a maximum error; and they define the priority level of each error variable.
In (15), $i_{\alpha ref}(t_{s+1})$ and $i_{\beta \mathrm{ref}}(t_{s+1})$, are the AC current references one sample time forward, $t_s+1$, to compensate for the processor calculation delay. To assure adjacent level voltage transition in the multilevel output voltage, thus minimizing the number of semiconductor commutations, only vectors adjacent to the vector in use at $t=t_s$ are analysed, since they need just the switching of two semiconductors per leg. The adjacent vectors verify $|\gamma_k(t_{s+1}) - \gamma_k(t_s)| < 2$ , with $k \in \{1, 2, 3\}$, in the 3 legs of the NPC converter.

### 2.3 Predictive fundamental frequency synchronization

The measurement of the fundamental frequency and phase of the network voltage is crucial in power quality applications. The AC voltage phase detector must be fast to ensure a

synchronization frame always in phase with the fundamental frequency of the network AC voltage. To achieve this a robust and fast phase detection/synchronization method together with fundamental frequency generation (for short interruptions) must be implemented. The phase and frequency recognition is hard to obtain from the AC network voltages when sags or interruptions occur. The synchronization must use the network AC waveforms, which can have amplitude and frequency variations, voltage sags/swells, short interruptions and distortion. The synchronization method must rapidly capture the phase of the network AC voltage after a short interruption, it must be robust to amplitude variations, and must handle AC voltages with unbalanced amplitudes.

To provide an optimal solution to the phase detection and fundamental frequency generation, an optimal predictive phase detection and fundamental frequency generation based on the dq Park transformation, is introduced.

The application of the Clarke-Concordia and the Park transformations to ideally balanced network AC voltages with synchronous frame, θ, can provide a zero quadrature, $U_q$, component. The synchronous frame, θ, can be obtained by finding the optimal value that results in a zero quadrature, $U_q$, AC voltage component.

To handle temporary total failures on the network AC voltage, the synchronization frame must be generated in a self-running mode at a constant frequency (50 Hz).

Applying the Clarke-Concordia to the network constant amplitude $U$ AC voltages and Park transformations with phase error $\Delta\theta(t_s)$, the direct component, $U_d(t_s)$, and the quadrature component, $U_q(t_s)$, calculated at the present sampling time, $t_s = k\Delta T$, are (Barros & Silva, 2010):

$$U_d(t_s) = \sqrt{\frac{3}{2}} U \cos\Delta\theta(t_s);\ U_q(t_s) = -\sqrt{\frac{3}{2}} U \sin\Delta\theta(t_s). \tag{16}$$

The phase error, $\Delta\theta(t_s)$, can be derived from the measured direct $U_d(t_s)$, and quadrature, $U_q(t_s)$, AC voltage components. At the next sampling time $t_{s+1} = (k+1)\Delta T$ the fundamental frequency has a phase variation of $\omega\Delta T$. Thus, the prediction of the phase error $\Delta\theta(t_{s+1})$ is

$$\Delta\theta(t_{s+1}) = \Delta\theta(t_s) - \omega\Delta T. \tag{17}$$

The prediction of the synchronous frame at the next sapling time, $\theta(t_{s+1})$, is obtained by subtracting the predicted phase error $\Delta\theta(t_{s+1})$ to the actual synchronous frame, $\theta(t_s)$,

$$\theta(t_{s+1}) = \theta(t_s) - \Delta\theta(t_{s+1}). \tag{18}$$

The Fig. 3 shows the predicted vector $\theta(t_{s+1})$ obtained from the phase error, $\Delta\theta(t_s)$, and the actual synchronous frame, $\theta(t_s)$, vectors.

The feedback control loop to obtain a synchronous frame, $\theta(t_{s+1})$, (Fig. 4) calculates the Clarke-Concordia and Park transformations to obtain the quadrature voltage component, $U_q(t_s)$, which is compared to its reference value, $U_{q\text{Ref}} = 0$. The $U_q(t_s)$ and $U_d(t_s)$ AC voltage components values feed an optimal predictive phase quadrature, (Barros & Silva, 2010), compensator that computes the phase error $\Delta\theta(t_s)$, using equations (16), generating the synchronous phase $\theta(t_{s+1})$, to obtain a quadrature voltage component, $U_q$, that ensures $U_{q\text{Ref}} = 0$.

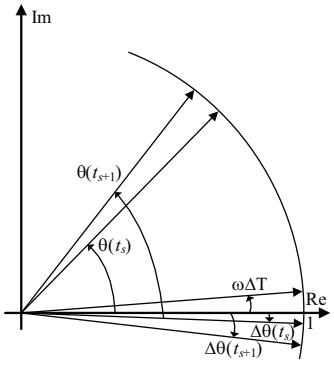


Fig. 3. Predictive synchronous frame vectors

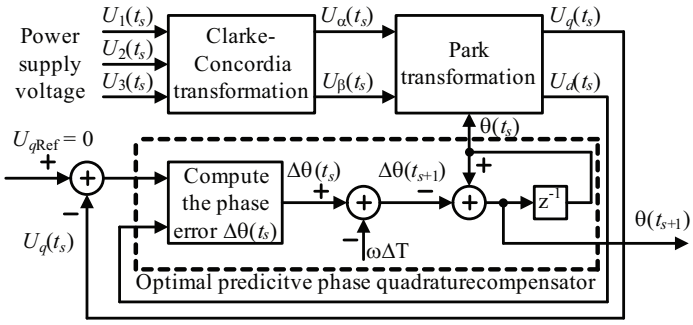


Fig. 4. Principle of optimal predictive phase and frequency detection based on dq Park transformation

Using the values of the voltage components $U_d(t_s)$ and $U_q(t_s)$ the optimal predictive phase quadrature compensator (Barros & Silva, 2010) predicts the optimal value of $\theta(t_{s+1})$ ($\cos[\theta(t_{s+1})]$ and $\sin[\theta(t_{s+1})]$) that minimizes the quadrature voltage component, $U_q$, of the network AC voltage, at the next sampling time $t_{s+1} = (k+1)\Delta T$,

$$\begin{aligned}\cos\left[\theta\left(t_{s+1}\right)\right] &= \cos\left[\theta\left(t_s\right)\right]\cos\left[\Delta\theta\left(t_{s+1}\right)\right] + \sin\left[\theta\left(t_s\right)\right]\sin\left[\Delta\theta\left(t_{s+1}\right)\right],\\ \sin\left[\theta\left(t_{s+1}\right)\right] &= \sin\left[\theta\left(t_s\right)\right]\cos\left[\Delta\theta\left(t_{s+1}\right)\right] - \cos\left[\theta\left(t_s\right)\right]\sin\left[\Delta\theta\left(t_{s+1}\right)\right].\end{aligned} \tag{19}$$

Where the phase error $\Delta\theta(t_{s+1})$, (17), at the next sampling time (and $\cos[\Delta\theta(t_{s+1})]$, $\sin[\Delta\theta(t_{s+1})]$) depends on the actual phase shift error $\Delta\theta(t_s)$ (as well as $\cos[\Delta\theta(t_s)]$, $\sin[\Delta\theta(t_s)]$). The actual phase shift error $\Delta\theta(t_s)$ can be related to the direct voltage component $U_d(t_s)$ (16), the quadrature voltage component, $U_q(t_s)$ (16), and the fundamental frequency phase variation $\omega\Delta T$ (Barros & Silva, 2010), as follows

$$\begin{aligned}\cos\left[\Delta\theta\left(t_{s+1}\right)\right] &= \cos\Delta\theta\left(t_s\right)\cos\left(\omega\Delta T\right) + \sin\Delta\theta\left(t_s\right)\sin\left(\omega\Delta T\right),\\ \sin\left[\Delta\theta\left(t_{s+1}\right)\right] &= \sin\Delta\theta\left(t_s\right)\cos\left(\omega\Delta T\right) - \cos\Delta\theta\left(t_s\right)\sin\left(\omega\Delta T\right).\end{aligned} \tag{20}$$

To handle the network AC voltage short interruptions, the synchronization frame must be generated in a self-running mode at a constant frequency (50 Hz) (Barros & Silva, 2010). The prediction of the self-running synchronous frame at the next sapling time, $\theta(t_{s+1})$, is

$$\theta(t_{s+1}) = \theta(t_s) + \omega\Delta T \ . \tag{21}$$

The optimal predictive phase quadrature compensator can be designed for unbalanced AC voltages, which is especially useful to detect the phase and frequency during unbalanced sags (Barros & Silva, 2010). Considering $U_1$, $U_2$, and $U_3$ the magnitudes of the unbalanced network AC voltage and applying the Clarke-Concordia and the Park transformations with synchronous frame, θ, the quadrature, $U_q(t_s)$, component (Barros & Silva, 2010), is

$$U_q(t_s) = \sqrt{\frac{1}{6}}\left(-\frac{\sqrt{3}}{2}U_2 + \frac{\sqrt{3}}{2}U_3\right)\cos 2\theta(t_s) + \sqrt{\frac{1}{6}}\left(-U_1 + \frac{U_2}{2} + \frac{U_3}{2}\right)\sin 2\theta(t_s) \ . \tag{22}$$

The quadrature, $U_q(t_s)$, component has second harmonic terms, $U_{2q}(t_s)$. The DC term, $U_{0q}(t_s)$ should be zero and can be obtained by subtracting the second harmonics term, $U_{2q}(t_s)$, to the quadrature component,

$$\begin{aligned} U_{0q}(t_s) &= U_q(t_s) - U_{2q}(t_s) = U_q(t_s) - \\ &-\sqrt{\frac{1}{6}}\left(-\frac{\sqrt{3}}{2}U_2 + \frac{\sqrt{3}}{2}U_3\right)\cos 2\theta(t_s) - \\ &-\sqrt{\frac{1}{6}}\left(-U_1 + \frac{U_2}{2} + \frac{U_3}{2}\right)\sin 2\theta(t_s) \\ &= 0 \end{aligned} \tag{23}$$

The optimal predictive phase quadrature compensator for unbalanced AC network voltages is designed to obtain the synchronous frame, θ, which results in zero DC quadrature component, $U_{0q}$, in a way similarly to the balanced AC network voltage fundamental frequency synchronization.

### 2.4 Evaluation of NPC multilevel converter predictive current controllers

To evaluate the performance of the optimal predictive AC current control algorithms and the capacitor voltage balancing in NPC converters, a DC source, $U_{dc}$ (120 V) with internal resistance 0.2 Ω, is connected in the DC side of the NPC converter (Fig. 1), the currents references, $i_{\alpha Ref}$ and $i_{\beta Ref}$, are obtained from DSP based lookup tables ($i_{ac}$ = 4 A), $U_L$ is obtained from 230/400V through a 400/230V transformer, and the following parameters were used: $C_1$ = 4.4 mF, 200 V, $C_2$ = 4.4 mF, 200 V, $L$ = 15.1 mH, $R$ = 0.1 Ω, $f_{ac}$ = 50 Hz ($T$ = 0.02 s and ω = 314.2 rad/s), $\rho_\alpha$ = 0.09 A², $\rho_\beta$ = 0.09 A², and $\rho_{UC}$ = 0.04 V².

Experimental results of the AC currents, $i_1$, $i_2$, and $i_3$, with $\Delta T$=28 μs and steady state operation (Fig. 5), show that they are nearly sinusoidal with very small ripple factor (less than 3%), and a total harmonic distortion (THD) lower than 1%. Applying a positive step (1 A to 4 A) in the AC current references (Fig. 5, at 5 ms) and a negative step (4 A to 1 A), at 45 ms the results show a fast dynamic response, with no overshoot, and no stationary error.

The optimal predictive controller also chooses the optimal vector that minimizes the capacitor voltage errors and these voltages are balanced (Fig. 6), with a mean error lower than 1%. Near perfect capacitor DC voltage balancing is obtained, while reducing AC current harmonic distortion.

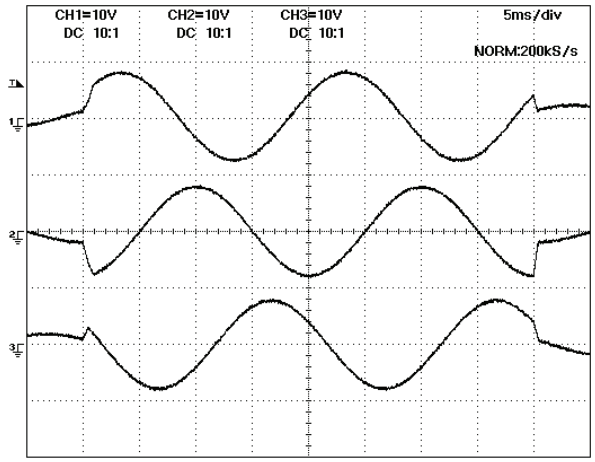


Fig. 5. Experimental results of sinusoidal AC currents, $i_1$, $i_2$, and $i_3$, with an amplitude step. $i_1$ has a displacement of 2 divisions and $i_3$ a displacement of –2 divisions (vertical – 5 A/Div and horizontal - 5 ms/Div)

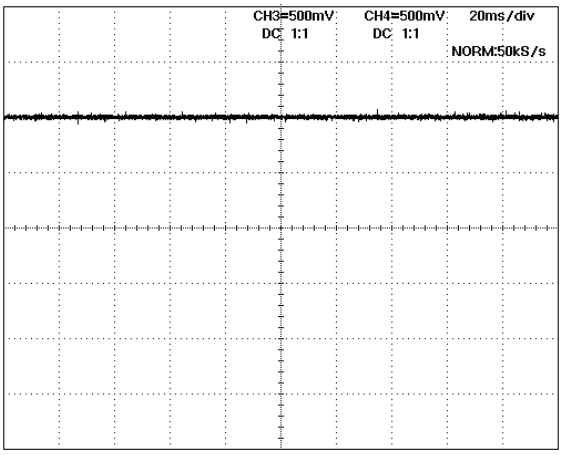


Fig. 6. Capacitor voltages, $U_{C1}$ and $U_{C2}$ (vertical - 10 V/Div and horizontal – 20 ms/Div)

The optimal predictive phase quadrature synchronization controller is tested during a short electrical network voltage interruption. The experimental results (Fig. 7a) show the electrical network voltage short interruption, $U_{L1}$, $U_{L2}$, and $U_{L3}$. The Fig. 7b show the phase θ of the optimal predictive synchronizer and a binary signal signalling that the electrical network voltages level voltage is lower than the minimum limit, $U_{dq\min}$. The results show that the

optimal predictive synchronizer is able to internally generate without interruptions a phase signal, at the fundamental frequency (50 Hz).

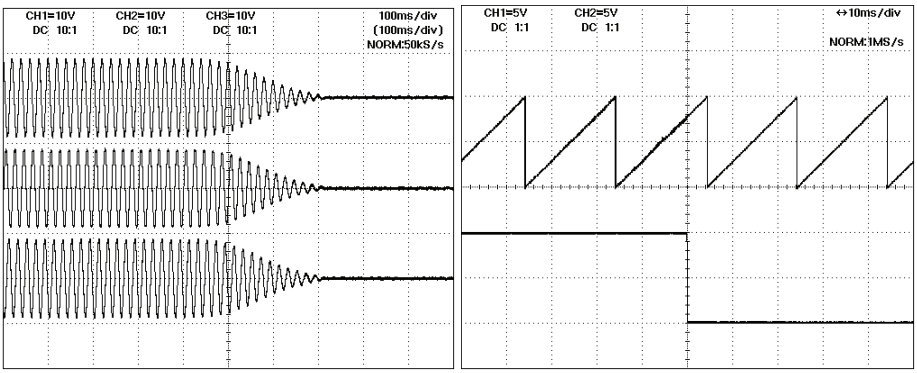


a) b)

Fig. 7. a) The electrical power network voltages, $U_{L1}$ + 740 V, $U_{L2}$ and $U_{L3}$ - 740 V. b) The phase θ and the signal showing the electrical power network voltages interruption (vertical 370 V/Div; π/Div and horizontal 100 ms/Div; 10 ms/Div)

## 3. Power quality applications of predictive controlled multilevel converters

Using the optimal predictive controllers and multilevel converters, power quality enhancing technologies are proposed, such as active power filters (APF) with reactive power compensation, unity power factor rectifiers (UPFR), and dynamic voltage restorers (DVR), which are tested using both MATLAB/SIMULINK simulations and a digital signal processor based laboratory prototype.

### 3.1 Active power filter

The NPC multilevel, connected as a shunt APF (Fig. 8), can be controlled to compensate the power factor and the AC line $i_{Lk}$ current harmonics introduced by non-linear loads such as three-phase bridge diode rectifier (Fig. 8). The NPC multilevel AC side is shunt connected to the electrical network voltages $U_{L1}$, $U_{L2}$, and $U_{L3}$ using three inductors, $L$, with resistive $R$ losses. The APF injects currents to cancel the harmonic components of the non-linear load currents. The DC voltage, $U_{dc}$, must be regulated and the capacitor voltages, $U_{C1}$ and $U_{C2}$, balanced.

The NPC converter APF model is obtained and the optimal predictive control of the electrical power network AC currents is derived from the principles outlined in section 2.1. Proportional integral (PI) type regulators, optimal predictive, sliding-mode and μ-synthesis are control methodologies proposed to regulate the DC capacitor voltage $U_{dc}$.

#### 3.1.1 Switched state-space model of the multilevel APF

Applying Kirchhoff laws to the multilevel converter APF (Fig. 8), the Clarke-Concordia transformation (5) and the Park transformation (8) the dynamic equations (24) of the AC line currents, $i_{Ld}$, and $i_{Lq}$, and the capacitor voltages, $U_{C1}$ and $U_{C2}$, can be written in function of the circuit parameters, as in 2.1.

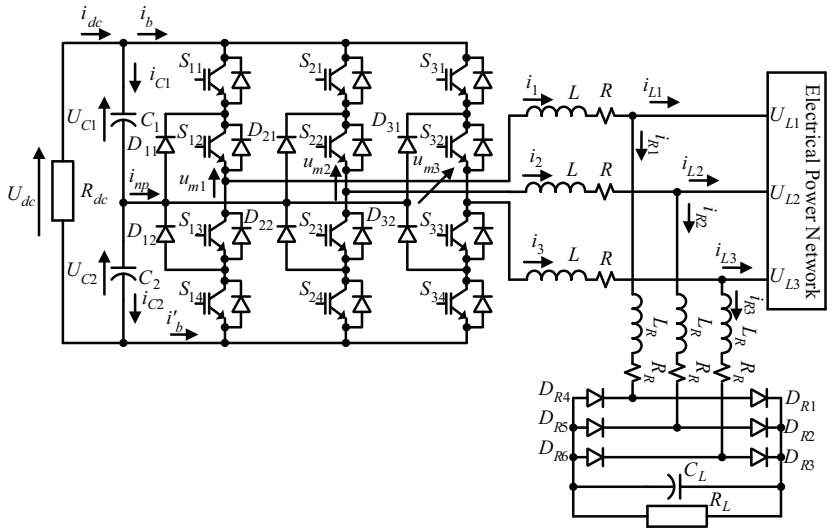


Fig. 8. NPC multilevel converter circuit, working as an active power filter

$$\begin{bmatrix} \frac{di_{Ld}}{dt} \\ \frac{di_{Lq}}{dt} \\ \frac{dU_{C1}}{dt} \\ \frac{dU_{C2}}{dt} \end{bmatrix} = \begin{bmatrix} -\frac{R}{L} & \omega & \frac{\Gamma_{1d}}{L} & \frac{\Gamma_{2d}}{L} \\ -\omega & -\frac{R}{L} & \frac{\Gamma_{1q}}{L} & \frac{\Gamma_{2q}}{L} \\ -\frac{\Gamma_{1d}}{C_1} & -\frac{\Gamma_{1q}}{C_1} & 0 & 0 \\ -\frac{\Gamma_{2d}}{C_2} & -\frac{\Gamma_{2q}}{C_2} & 0 & 0 \end{bmatrix} \begin{bmatrix} i_{Ld} \\ i_{Lq} \\ U_{C1} \\ U_{C2} \end{bmatrix} + \begin{bmatrix} -\frac{1}{L} & 0 & 0 \\ 0 & -\frac{1}{L} & 0 \\ 0 & 0 & \frac{1}{C_1} \\ 0 & 0 & \frac{1}{C_2} \end{bmatrix} \begin{bmatrix} U_{Ld} \\ U_{Lq} \\ i_{dc} \end{bmatrix} + \\ + \begin{bmatrix} -\frac{R}{L} & \omega & -1 & 0 \\ -\omega & -\frac{R}{L} & 0 & -1 \\ -\frac{\Gamma_{1d}}{C_1} & -\frac{\Gamma_{1q}}{C_1} & 0 & 0 \\ -\frac{\Gamma_{2d}}{C_2} & -\frac{\Gamma_{2q}}{C_2} & 0 & 0 \end{bmatrix} \begin{bmatrix} i_{Rd} \\ i_{Rq} \\ \frac{di_{Rd}}{dt} \\ \frac{di_{Rq}}{dt} \end{bmatrix} \tag{24}$$

The DC voltage, $U_{dc}$, dynamic equation is obtained directly from (24) since $U_{dc} = U_{C1} + U_{C2}$,

$$\frac{dU_{dc}}{dt} = -\left(\frac{\Gamma_{1d}}{C_1} + \frac{\Gamma_{2d}}{C_2}\right) i_{Ld} - \left(\frac{\Gamma_{1q}}{C_1} + \frac{\Gamma_{2q}}{C_2}\right) i_{Lq} - \\ -\left(\frac{\Gamma_{1d}}{C_1} + \frac{\Gamma_{2d}}{C_2}\right) i_{Rd} - \left(\frac{\Gamma_{1q}}{C_1} + \frac{\Gamma_{2q}}{C_2}\right) i_{Rq} + \left(\frac{1}{C_1} + \frac{1}{C_2}\right) i_{dc} \tag{25}$$

This DC voltage quasi-linear model, $U_{dc}$, is suitable to design a linear predictive controller to regulate the DC voltage of the APF.

### 3.1.2 Predictive equations for AC line currents and DC capacitor voltages

The AC current and DC voltage predictive optimal controllers are designed to choose the best output voltage vector able to minimize the AC line current, $i_{L\alpha}$ and $i_{L\beta}$ errors, $U_{dc}$ voltage regulation error and the unbalancing of DC capacitor voltages, $U_{C1}$ and $U_{C2}$. The obtained αβ converter model is solved (like in section 2.2.1) to predict the state variable values at the next sampling period, for all the 27 available vectors.

$$\begin{aligned} i_{Lx}(t_{s+1}) \approx i_{Lx}(t_s) + i_{Rx}(t_s) - i_{Rx}(t_{s+1}) - \frac{R}{L}\Delta T i_{Lx}(t_s) - \frac{R}{L}\Delta T i_{Rx}(t_s) + \\ + \frac{\Gamma_{1x}}{L}\Delta T U_{C1}(t_s) + \frac{\Gamma_{2x}}{L}\Delta T U_{C2}(t_s) - \frac{\Delta T}{L}U_{Lx}(t_s) \end{aligned} \tag{26}$$

$$\begin{aligned} U_{C1}(t_{s+1}) - U_{C2}(t_{s+1}) \approx U_{C1}(t_s) - U_{C2}(t_s) + (\Gamma_{2\alpha} - \Gamma_{1\alpha})\frac{\Delta T}{C}\left[i_{L\alpha}(t_s) + i_{R\alpha}(t_s)\right] + \\ + (\Gamma_{2\beta} - \Gamma_{1\beta})\frac{\Delta T}{C}\left[i_{L\beta}(t_s) + i_{R\beta}(t_s)\right] \end{aligned} \tag{27}$$

### 3.1.3 Quadratic cost functional definition

In the APF the NPC multilevel converter is operating as a current source, controlling the two AC line currents $i_{L\alpha}(t)$, $i_{L\beta}(t)$, and the capacitive unbalance $U_{C1}(t)$-$U_{C2}(t)$, thus the quadratic cost functional (14) is rewritten to minimize the AC line currents errors, $e_\alpha(t_{s+1}) = i_{L\alpha Ref}(t_{s+1}) - i_{L\alpha}(t_{s+1})$ and $e_\beta(t_{s+1}) = i_{L\beta Ref}(t_{s+1}) - i_{L\beta}(t_{s+1})$, and the capacitor voltage difference, $e_{UC}(t_{s+1}) = U_{C1}(t_{s+1}) - U_{C2}(t_{s+1})$. The $i_{L\alpha Ref}(t_{s+1})$ and $i_{L\beta Ref}(t_{s+1})$, are the AC line current references one sample time forward, $t_{s+1}$. These current references will be computed to ensure near unity power factor and to regulate the $U_{dc}$ voltage.

### 3.1.4 Multilevel converter APF optimal predictive controller

The block diagram of the multilevel converter APF with the optimal controller (Fig. 9a) includes as inputs, the states of the multilevel converter switches (all the vectors to be tested), $\gamma_1(t_s)$, $\gamma_2(t_s)$, and $\gamma_3(t_s)$, the sampled capacitor voltages, $U_{C1}(t_s)$ and $U_{C2}(t_s)$, the AC line current references, one sampling time forward, $i_{L\alpha Ref}(t_{s+1})$ and $i_{L\beta Ref}(t_{s+1})$, and the AC currents, $i_{L1}(t_s)$, $i_{L2}(t_s)$, $i_{L3}(t_s)$, $i_{R1}(t_s)$, $i_{R2}(t_s)$, and $i_{R3}(t_s)$, sampled and transformed to αβ coordinates, $i_{L\alpha}(t_s)$, $i_{L\beta}(t_s)$, $i_{R\alpha}(t_s)$, and $i_{R\beta}(t_s)$. The controller makes use of these inputs to compute the optimal vector, in order to apply it to the NPC converter, at the next sampling interval. Adjacent level voltage transition is also ensured.

### 3.1.5 Active power filter current reference generation and power flow control

The generation of the AC line current references, $i_{Ld Ref}$ and $i_{Lq Ref}$, for the active power filter must assure that the AC line currents are sinusoidal, the power factor is near unity and the DC voltage is regulated.

A linear optimal predictive regulator is here designed to generate references, $i_{Ld Ref}$ and $i_{Lq Ref}$, able to cancel the mean value of the DC voltage error, $e_{Udc}(t) = U_{dc Ref}(t) - U_{dc}(t)$, during the time interval $T_{Udc}$ (28).

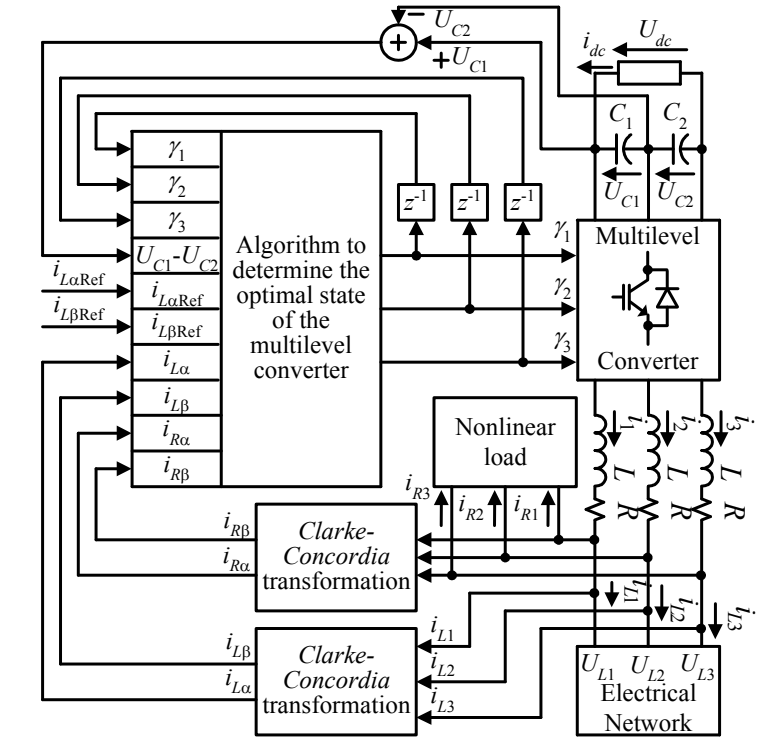


(a)

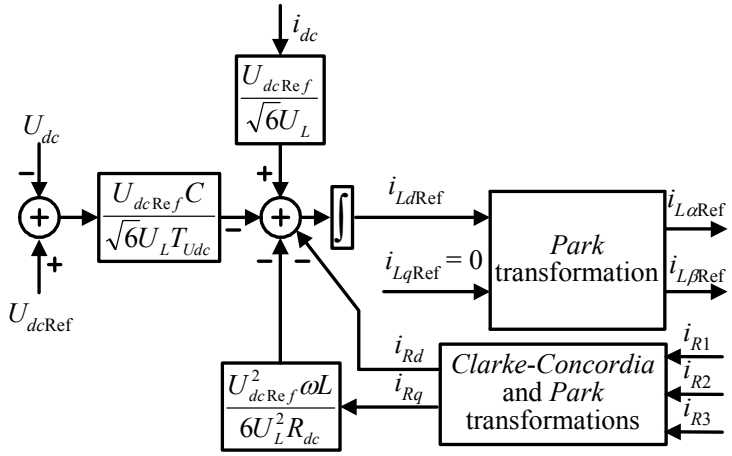


(b)

Fig. 9. Feedback system of the multilevel converter APF with predictive optimal controller. (a) NPC multilevel optimal predictive controller. (b) APF current reference generation

$$\overline{e_{Udc}}(t)=\frac{1}{T_{Udc}}\int_{T_{Udc}} e_{Udc}(t)dt=\frac{1}{T_{Udc}}\int_{T_{Udc}} U_{dcRef}(t)-U_{dc}(t)dt=0 \tag{28}$$

To obtain a quasi-unity power factor the AC line current must be in phase with the AC line voltage, forcing $i_{LqRef}$ = 0. Using the dynamic equation of the DC voltage (25) in (28), assuming that the optimal predictive controller forces the $i_{Ld}$=$i_{LdRef}$ and $i_{LqRef}$ = 0, the optimal predictive control law of $i_{LdRef}$ is:

$$i_{LdRef}(t)\approx-\overline{i_{Rd}}(t)-\frac{U_{dcRef}C}{\sqrt{6}U_L}\frac{\overline{U_{dcRef}}(t)-\overline{U_{dc}}(t)}{T_{Udc}}-\frac{U_{dcRef}^2\omega L}{6U_L^2R_{dc}}\overline{i_{Rq}}(t)+\frac{U_{dcRef}\omega L}{\sqrt{6}U_L}\overline{i_{dc}}(t). \tag{29}$$

Where $T_{Udc}$ is the time interval used to compute the mean value of the DC voltages, $U_{dc}$ and $U_{dcRef}$, the DC current, $i_{dc}$, and the non-linear currents, $i_{Rd}$ and $i_{Rq}$. $U_L$ is the AC line voltage amplitude and $\omega$ is the fundamental angular frequency. The time interval $T_{Udc}$ must be much larger than the period, $T$, of AC line currents ($T_{udc}$ >> $T$) to maintain the AC line currents sinusoidal, (the time constant $R_{dc}C$ is of no concern since $R_{dc}$ represents the safety discharge resistors of the capacitors, $TU_{dc}$ << $R_{dc}C$). Therefore, the active power drawn from the AC network just compensates the converter losses. In (29) the switching variables, $\Gamma_{1d}$+$\Gamma_{2d}$ and $\Gamma_{1q}$+$\Gamma_{2q}$, were obtained similarly as in (Silva, 1999) and are given in (30).

$$\Gamma_{1d}+\Gamma_{2d}\approx\frac{\sqrt{6}U_L}{U_{dcRef}};\ \Gamma_{1q}+\Gamma_{2q}\approx\frac{2\omega LU_{dcRef}}{\sqrt{6}U_LR_{dc}} \tag{30}$$

In the control of the APF, the DC voltages ($U_{dc}$) and currents ($i_{dc}$, $i_{R1}$, $i_{R2}$, and $i_{R3}$) are sampled to generate the AC line current references (Fig. 9b), which are applied to the optimal predictive controller of the multilevel converter (Fig. 9a) to force the AC line currents to follow their references.

The regulation of DC capacitor voltage can also be done using other regulators such as (Barros & Silva, 2008): PI-type regulators (31), sliding-mode (32), and μ-synthesis (33).

The DC PI regulator parameters, $K_{pUdc}$ and $K_{iUdc}$, (31), depend on two system parameters, $\omega_n$ and $\zeta$, which characterize the second-order system closed loop behaviour. The damping factor, $\zeta$, is usually chosen with values close to 0.707, to avoid severe overshoots in the step response to the voltage DC reference, $U_{dcRef}$ (or to minimize the integral of time multiplied by absolute error – the ITAE criterion). The natural frequency $\omega_n$ should be a much lower frequency than the AC voltage frequency, $\omega_n$ << $\omega$ ($\omega$=2π50 rad/s), so that the amplitude of the currents of the electrical power network shows much slower variations than the AC currents frequency (50 Hz).

$$\begin{aligned} i_{LdRef}&=\left(k_{pUdc}+\frac{k_{iUdc}}{s}\right)\left(U_{dcRef}-U_{dc}\right);\\ K_{pUdc}&=\frac{U_{dcRef}-U_{dcRef}\zeta\omega_nR_{dc}C}{\sqrt{6}U_LR_{dc}};\\ K_{iUdc}&=-\frac{U_{dcRef}\omega_n^2C}{2\sqrt{6}U_L}. \end{aligned} \tag{31}$$

In the sliding mode control law (32), the time constant $\beta_{eUdc}$ defines the role of the instantaneous error in the DC voltage control variable, $i_{Ld\text{Ref}}$. In the APF, the control variables, that regulate the DC voltage, are the network AC current amplitudes, which must be almost sinusoidal and therefore can not have abrupt variations. The time constant $\beta_{eUdc}$ should be much lower than the integration period ($\beta_{eUdc} << T_{Udc}$) so that AC current amplitudes are slowly time variant.

$$\begin{aligned} i_{Ld\text{Re}f}(t) \approx -\overline{i_{Rd}}(t) - \frac{\beta_{eUdc}}{T_{Udc}} \frac{U_{dc\text{Re}f} C}{\sqrt{6} U_L} \frac{U_{dc\text{Re}f}(t) - U_{dc}(t)}{T_{Udc}} - \\ - \frac{U_{dc\text{Re}f} C}{\sqrt{6} U_L} \frac{\overline{U_{dc\text{Re}f}}(t) - \overline{U_{dc}}(t)}{T_{Udc}} - \\ - \frac{U_{dc\text{Re}f}^2 \omega L}{6 U_L^2 R_{dc}} \overline{i_{Rq}}(t) + \frac{U_{dc\text{Re}f}}{\sqrt{6} U_L} \overline{i_{dc}}(t) \end{aligned} \tag{32}$$

The overall structure to synthesis the μ-synthesis compensator (33), with the methodology based on structured singular values, having a general model, $P(s)$ and a dynamics of uncertainty, $\Delta(s)$, was implemented in MATLAB with the μ–Synthesis tool. A compensator (33) was obtained to ensure robust stability and robust performance for the APF (Barros et al., 2005). The values of the parameters, components, and uncertainties used to design the compensator are (Barros & Silva, 2008): $C_1 = C_2 = 4.4$ mF, $C_L = 1$ mF, $L = 15$ mH, $L_R = 1$ mH, $R = 0.7\ \Omega$, $R_{dc} = 1$ kΩ, $R_L = 10\ \Omega$, and $R_R = 0.1\ \Omega$.

$$i_{Ld\text{Re}f} = \frac{-0.097\left(s - 1.4\times10^4\right)\left(s + 3269\right)\left(s^2 + 36.5s + 548.6\right)}{\left(s + 306.8\right)\left(s + 2.4\right)\left(s + 0.33\right)\left(s^2 + 275.3s + 4.7\times10^4\right)}\left(U_{dc\text{Re}f} - U_{dc}\right) \tag{33}$$

### 3.1.6 Simulation and experimental results

The shunt connected multilevel APF (Fig. 8) is controlled to compensate the load current harmonics and to regulate the power factor at unity. The AC current references of the APF are generated to regulate the mean value of the DC voltage, $U_{dc\text{Ref}} = 240$ V, the power factor and the AC line currents.

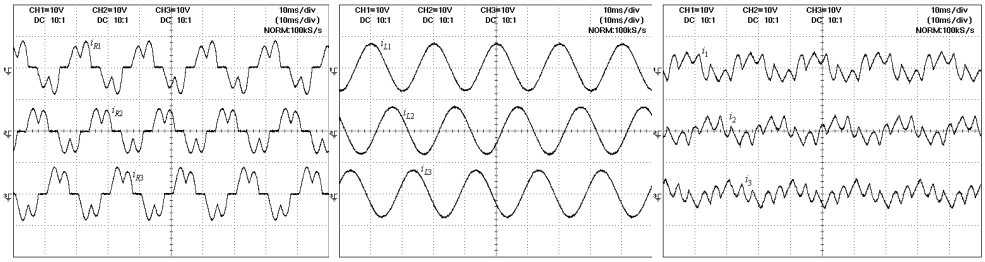

a) b) c)

Fig. 10. Experimental results of: a) the non-linear currents, $i_{R1}$, $i_{R2}$, and $i_{R3}$; b) the AC line currents, $i_{L1}$, $i_{L2}$, and $i_{L3}$; c) the output currents, $i_1$, $i_2$, and $i_3$ of the active power filter. $i_{R1}$ , $i_{L1}$, and $i_1$ have a displacement of 2 divisions and $i_{R3}$, $i_{L3}$, and $i_3$ a displacement of –2 divisions (vertical - 12 A/Div and horizontal - 10 ms/Div).

The experimental results of the rectifier non-linear currents, $i_{R1}$, $i_{R2}$, and $i_{R3}$ (Fig. 10a), show that the THD is about 36% and the power factor is 0.91. The multilevel APF injects currents (Fig. 10c) to cancel the current harmonic components of this non-linear load. The THD of AC line currents is reduced from 36% to nearly 1% (Fig. 10b).
The DC voltage, $U_{dc}$ (Fig. 11a) shows that the DC voltage follows it references ($U_{dc\text{Ref}}$ = 240 V) with almost no steady state error (0.3%).
Figure 11b shows the experimental results of the AC line currents, $-i_{L1}$ and $-i_{L2}$, simultaneously with the AC line voltages, $U_{L1}$ and $U_{L2}$. The results indicate that the AC line voltage and the AC line currents are sinusoidal and in phase, showing that the power factor is near unity. The power factor was improved from 0.910 (without APF) to 0.997 (with APF). The optimization of the multilevel current control improves the performance of the active power filter performance, by reducing the total harmonic distortion of AC line currents.

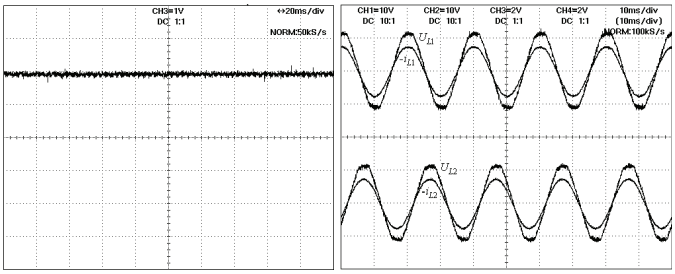


a) b)

Fig. 11. a) Experimental results of the DC voltage, $U_{dc}$, of the active power filter (vertical - 40 V/Div and horizontal - 20 ms/Div). b) The AC line currents, $-i_{L1}$, and $-i_{L2}$ (vertical – 12 A/Div), and the AC line voltages, $U_{L1}$ and $U_{L2}$ (vertical - 40 V/Div), of the active power filter. $i_{L1}$ and $U_{L1}$ have a displacement of 2 divisions and $i_{L2}$ and $U_{L2}$ a displacement of –2 divisions (horizontal - 10 ms/Div)

### 3.2 Unity power factor rectifier

The UPFR is based on the three-phase NPC multilevel converter. The optimal predictive controller enforces the AC currents to be almost sinusoidal and in phase with the electrical power network. Therefore, the electrical power network sees the rectifier load almost like a pure resistance avoiding current (and voltage) distortion, which improves power quality.
The multilevel rectifier has two control feedback loops: a slow and external for the control of DC voltage (a PI controller is used) and the internal current control loop (predictive controller) that also balances DC capacitors voltages. The predictive optimum controller minimizes the ripple factor and total harmonic distortion of input currents of UPFR. The amplitudes of the AC current references are obtained using the PI controller of the rectifier DC voltage.
The predictive methodology is compared with a fast non-linear method (sliding-mode) to evaluate the performance improvement resulting from the use of optimal predictive control of multilevel converter, ensuring that experiments are done under the same conditions and with the same PI controller parameters to control the DC voltage.

#### 3.2.1 Switched state-space multilevel UPFR model

To operate as rectifier, the three-phase NPC multilevel converter has the three legs connected to the electrical power network, through coupling inductors, $L$ (with loss resistor, $R$), and

the load is connected to the DC side seeing the sum of the voltages of the capacitors $C_1$ and $C_2$ ( Fig. 12). The main power flow direction is from electrical power network to the DC load. Yet, the UPFR is bidirectional and can transfer power from the DC side to the AC side.

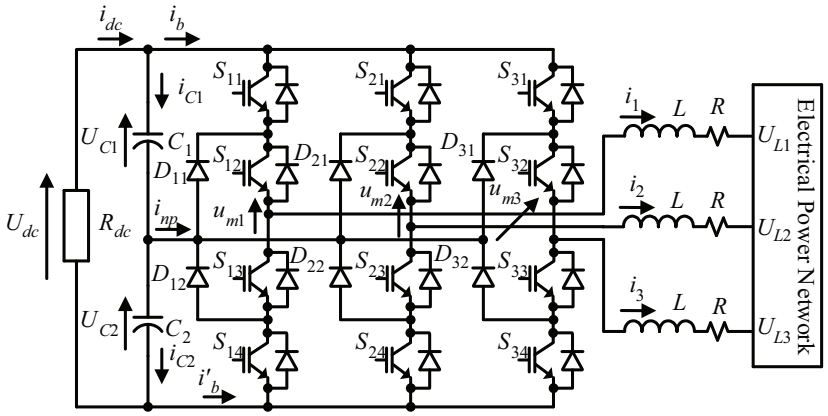


Fig. 12. Multilevel NPC rectifier with three legs

The dynamic equations of the AC currents and the capacitors voltage, $U_{C1}$ and $U_{C2}$ are similar to the NPC converter in section 2.1. Since $U_{dc} = U_{C1} + U_{C2}$, the dynamic equation of the rectifier DC voltage, $U_{dc}$, is obtained directly from (9),

$$\frac{dU_{dc}}{dt} = -\left(\frac{\Gamma_{1d}}{C_1} + \frac{\Gamma_{2d}}{C_2}\right) i_d - \left(\frac{\Gamma_{1q}}{C_1} + \frac{\Gamma_{2q}}{C_2}\right) i_q + \left(\frac{1}{C_1} + \frac{1}{C_2}\right) i_{dc} \,. \tag{34}$$

The design of the PI linear controller for the rectifier DC voltage is based on the dq coordinates dynamic equation (34), since it is time invariant at steady state operation.

### 3.2.2 Predictive control of AC line currents and DC capacitor voltages

The dynamic equations of the state space variables in multilevel rectifier are similar to the dynamic equations of the multilevel inverter (6). The design of the optimal predictive controller for AC line currents is done as in Section 2.2 (multilevel current inverter). In the multilevel converter, working as inverter, the current references, $i_{\alpha\text{Ref}}$ and $i_{\beta\text{Ref}}$, were obtained from lookup tables. However, in the rectifier mode, the current references must be derived from the voltage regulator, which in each moment computes the current references to ensure that the voltage DC, $U_{DC}$, follow its reference, $U_{dc\text{Ref}}$.

### 3.2.3 UPFR current reference generation and DC voltage control

To ensure near unity power factor, the AC currents at the input of the multilevel rectifier must be sinusoidal and in phase with the voltages. The DC voltage PI controller generates the AC references current, $i_{d\text{Ref}}$ and $i_{q\text{Ref}}$, of the multilevel converter for the DC voltage, $U_{dc}$, to follow its reference, $U_{dc\text{Ref}}$ without steady-state errors. The dynamics of the DC voltage rectifier (34) is similar to the dynamic DC voltage of the APF (25). Therefore, the design of the DC voltage regulator rectifier was made with a PI compensator with the same parameters of the APF (31).

### 3.2.4 Simulation and experimental results

In UPFR simulations and experiments the parameters have the following values: $C_1$ = 20 mF, $C_2$ = 18.6 mF, $R_{dc}$ = 100 Ω, $R$ = 0.1 Ω, $L$ = 15.5 mH, $U_{dc\mathrm{Ref}}$ = 100 V, $U_{L\mathrm{RMS}}$ = 24 V, $f_{ac}$ = 50 Hz, $\Delta T$ = 28 μs, $\zeta$ = 0.71, $\omega_n$ = 4 rad/s, $\rho_\alpha$ = 0.09 A², $\rho_\beta$ = 0.09 A², and $\rho_{UC}$ = 0.04 V².

In steady-state operation the experimental and simulation results of the rectified DC voltage, $U_{dc}$, (Fig. 13) show that this voltage follows the reference, $U_{dc\mathrm{Ref}}$, without stationary error.

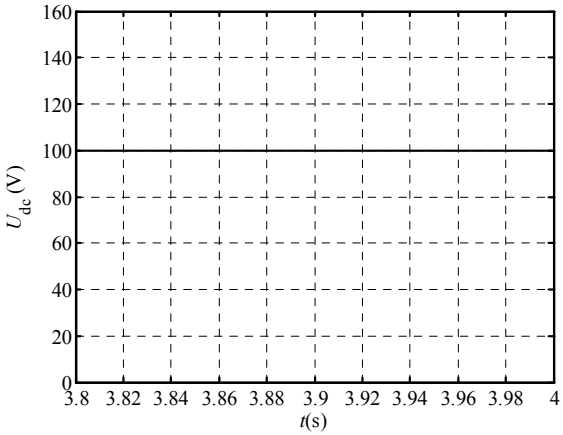


(a) Simulation results

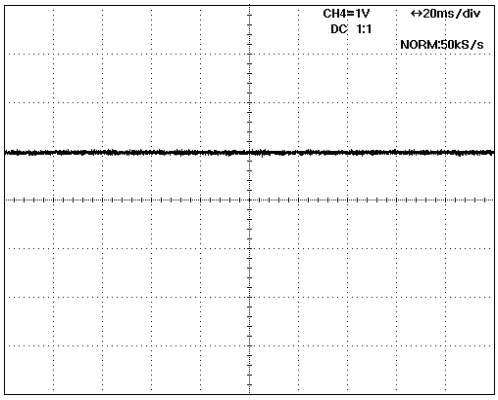


b) Experimental results

Fig. 13. $U_{dc}$ voltage in steady state operation. Each vertical division is 20 V/Div

The line AC currents, at the input of the multilevel rectifier, (Fig. 14b) are quasi sinusoidal, as is needed, with an rms ripple error near to 1% (0.02 A) having an expressive improvement comparatively to the sliding mode controller (Fig. 14a), which have an rms ripple error of approximately 9% (0.1 A).

The rms error of the electric network voltage, $U_{L1}$, $U_{L2}$, and $U_{L3}$, is about 7% (3.5 V). The AC line currents are in phase with the electric network voltage (Fig. 14), showing that both controllers have a near unity power factor.

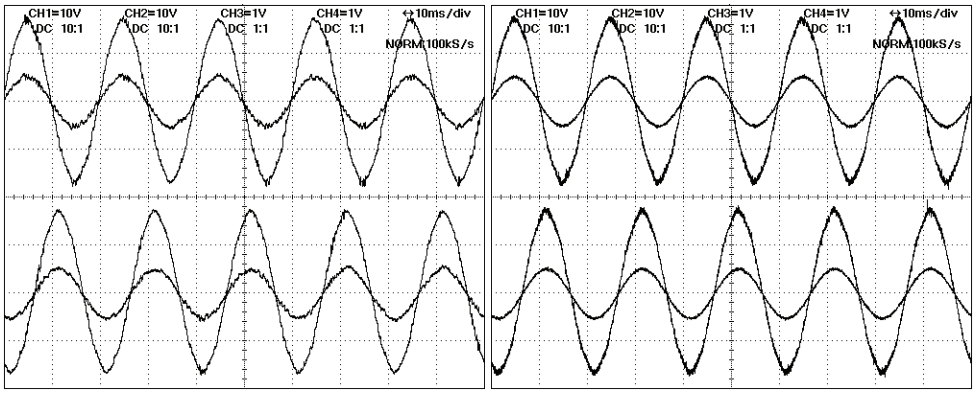


a) Sliding mode controller b) Optimal predictive controller

Fig. 14. AC currents, $-i_1$ and $-i_2$, and AC line voltages, $U_{L1}$ and $U_{L2}$, in steady state operation. The AC current vertical division is 5 A/Div and the AC voltage vertical division is 20 V/Div

### 3.3 Dynamic voltage restorer

Dynamic voltage restorers are mainly used to protect sensitive loads from the electrical network voltage disturbances, such as sags or swells, and could be used to reduce flicker and harmonic distortion of AC voltages (acting as series active filters). Voltage sags are abrupt reductions (between 10% and 99%) in the AC voltage root mean square value, lasting less than 60 seconds.

The DVR is here designed using optimal predictive output voltage controllers to ensure sensitive load AC sinusoidal voltages with constant amplitude, without interruptions and unbalances, while reducing the AC voltage THD, even during the presence of sags, short interruptions and high values of THD. The pre-sag compensation is used to restore the existing amplitude voltage and phase prior to the voltage short interruption, and the in-phase compensation is used to mitigate sags, minimizing the DVR voltage amplitude. The sensitive load AC voltage waveform quality is improved using the designed optimal predictive NPC based DVR. The synchronous dq frame predictive controller of the output AC voltage, able to mitigate AC voltage disturbances is designed and it is compared to a synchronous dq frame PI controller and asynchronous (P+resonant) proportional integral controller in simulation and experimental results. Using the state-space model of the three-phase NPC converter, the obtained optimal predictive controller in addiction reduces the THD of the AC voltages. The optimal predictive phase quadrature synchronizer (section 2.3) detects the phase of the AC network voltages and generates the fundamental frequency.

#### 3.3.1 Optimal predictive controller of the sensitive load AC voltage

The control system of DVR uses an outer loop for the AC load voltage control, which generates the current references, $i_{\alpha Ref}$ and $i_{\beta Ref}$, for the inner predictive AC current loop.

The structure of the optimal predictive multilevel DVR showing the interconnection of sub-systems and feedback control loops is represented in Fig. 15. The optimal predictive outer loop controller of the AC sensitive load voltages generates, through a limiter, the current

references, $i_{\alpha Ref}$ and $i_{\beta Ref}$, for the inner AC current loop optimal predictive controllers (reported in section 3.3.4). An equivalent DVR model connected to an AC network is derived next to design the outer loop controllers, including the optimal predictive controller for the load sensitive AC voltages.

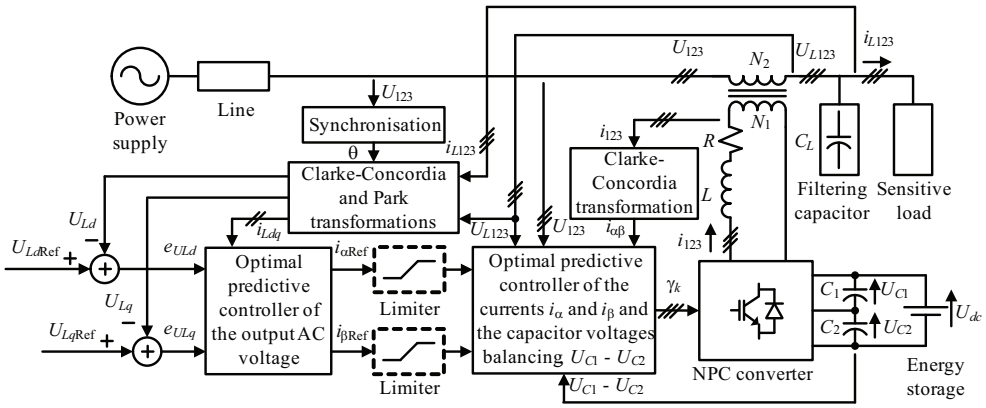


Fig. 15. Optimized feedback system of the DVR to improve the power quality of the output AC voltage of critical sensitive loads

The AC network voltages ($U_1$, $U_2$, and $U_3$) are represented using the equivalent network model with line inductances ($L_{Line}$) and equivalent loss resistors ($R_{Line}$) (Fig. 16). One three phase transformer with 3 separated secondary windings, each one series connected with each line voltage, is used to series inject the compensation voltage for the critical load. The filtering capacitors $C_L$ (Fig. 16) are placed on the line-side to obtain high control bandwidth while reducing the NPC converter high frequency switching harmonics.

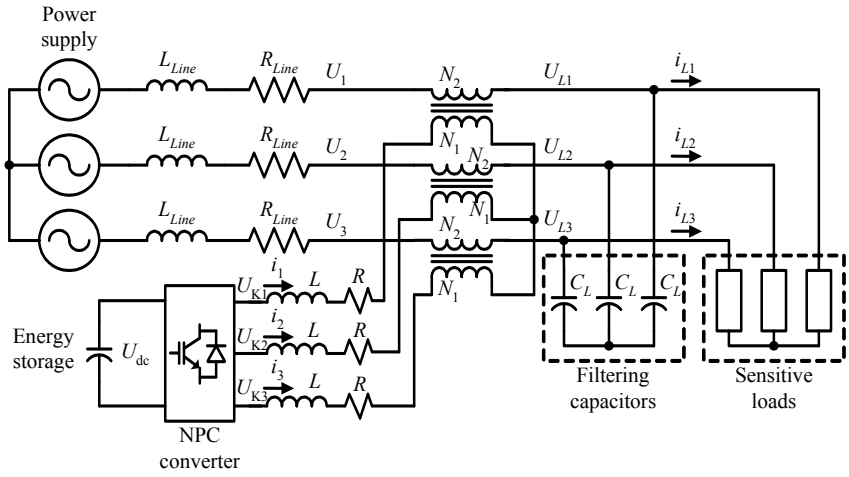


Fig. 16. Three-phase DVR simplified power circuit

Assuming balanced operation and using Kirchhoff laws in the DVR circuit (Fig. 16), the dynamic equations (35) of the sensitive load AC voltages ($U_{L1}$, $U_{L2}$, and $U_{L3}$), can be written as functions of the circuit parameters (filter capacitor $C_L$ and transformer ratio $n$=$N_2/N_1$).

$$\frac{dU_{Lj}}{dt} = \frac{1}{nC_L} i_j - \frac{1}{C_L} i_{Lj}; \quad j = 1,2,3 \tag{35}$$

These equations (35) are suitable to design the outer loop controllers for $U_{L1}$, $U_{L2}$, and $U_{L3}$ voltages. Their control inputs are the NPC converter output AC currents $i_1$, $i_2$, and $i_3$. From the control viewpoint, the load currents, $i_{L1}$, $i_{L2}$, and $i_{L3}$, are considered as disturbances.
For control purposes, the isolated neutral output AC voltages, can be advantageously written in αβ and then in dq coordinates. Using the Clarke-Concordia transformation the αβ coordinates model of the output AC voltage (35), is (36).

$$\begin{bmatrix} \frac{dU_{L\alpha}}{dt} \\ \frac{dU_{L\beta}}{dt} \end{bmatrix} = \begin{bmatrix} \frac{1}{nC_L} & 0 \\ 0 & \frac{1}{nC_L} \end{bmatrix} \begin{bmatrix} i_\alpha \\ i_\beta \end{bmatrix} + \begin{bmatrix} -\frac{1}{C_L} & 0 \\ 0 & -\frac{1}{C_L} \end{bmatrix} \begin{bmatrix} i_{L\alpha} \\ i_{L\beta} \end{bmatrix} \tag{36}$$

Using the Park transformation in (36), the model of the output AC voltage (37) in dq coordinates is obtained.

$$\begin{bmatrix} \frac{dU_{Ld}}{dt} \\ \frac{dU_{Lq}}{dt} \end{bmatrix} = \begin{bmatrix} 0 & \omega \\ -\omega & 0 \end{bmatrix} \begin{bmatrix} U_{Ld} \\ U_{Lq} \end{bmatrix} + \begin{bmatrix} \frac{1}{nC_L} & 0 \\ 0 & \frac{1}{nC_L} \end{bmatrix} \begin{bmatrix} i_d \\ i_q \end{bmatrix} - \begin{bmatrix} \frac{1}{C_L} & 0 \\ 0 & \frac{1}{C_L} \end{bmatrix} \begin{bmatrix} i_{Ld} \\ i_{Lq} \end{bmatrix} \tag{37}$$

An optimal predictive controller of the sensitive load AC voltages intends to predict the value of the multilevel current references needed to minimize the errors of load AC voltages (relatively to their references). At time step $t_s = k\Delta T_{ULdq}$ ($\Delta T_{ULdq}$ is the voltage loop sampling step) the prediction of the multilevel current references for the next sampling step $t_{s+1} = (k+1)\Delta T_{ULdq}$, $i_{d\mathrm{Ref}}(t_{s+1})$ and $i_{q\mathrm{Ref}}(t_{s+1})$ (38), is obtained trough inversion of the dynamic equations of the sensitive load AC voltages (37), considering that the actual ($t_s = k\Delta T_{ULdq}$) sampled load voltages $U_{Ld}(t_s)$ and $U_{Lq}(t_s)$, must follow their references $U_{Ld\mathrm{Ref}}(t_{s+1})$ and $U_{Lq\mathrm{Ref}}(t_{s+1})$ within one voltage loop sampling time $\Delta T_{ULdq}$ (the next sampling step).

$$\begin{aligned} i_{d\mathrm{Ref}(t_{s+1})} &= nC_L \frac{U_{Ld\mathrm{Ref}(t_{s+1})} - U_{Ld(t_s)}}{\Delta T_{ULdq}} - nC_L \omega U_{Lq(t_s)} + n i_{Ld(t_s)}; \\ i_{q\mathrm{Ref}(t_s+1)} &= nC_L \frac{U_{Lq\mathrm{Ref}(t_s+1)} - U_{Lq(t_s)}}{\Delta T_{ULdq}} + nC_L \omega U_{Ld(t_s)} + n i_{Lq(t_s)} \end{aligned} \tag{38}$$

These predictive equations, (38), are discrete feedback control laws (sampling time $\Delta T_{ULdq}$ = 360 μs) for the sensitive load AC voltages in dq coordinates, giving the reference

currents $i_{d\mathrm{Ref}}(t_{s+1})$ and $i_{q\mathrm{Ref}}(t_{s+1})$ needed to track the critical load reference voltages, $U_{Ld\mathrm{Ref}}(t_{s+1})$ and $U_{Lq\mathrm{Ref}}(t_{s+1})$.

### 3.3.2 Synchronous dq frame PI controller of the output AC voltage

The design of the PI controller can be advantageously made by decoupling the cross coupling terms on the dynamic equations of the sensitive load AC voltage in (37). The PI control laws of $i_{d\mathrm{Ref}}$ and $i_{q\mathrm{Ref}}$ (39), are functions of the output AC voltage errors and the $K_p$ and $K_I$ parameters:

$$\begin{aligned} i_{d\mathrm{Re}f} &= K_P\left(U_{LdRef} - U_{Ld}\right) + K_I\int\left(U_{LdRef} - U_{Ld}\right)dt - nC_L\omega U_{Lq}; \\ i_{q\mathrm{Re}f} &= K_P\left(U_{LqRef} - U_{Lq}\right) + K_I\int\left(U_{LqRef} - U_{Lq}\right)dt + nC_L\omega U_{Ld}. \end{aligned} \tag{39}$$

The parameters, $K_P = 2n\zeta\omega_n C_L$ and $K_I = C_L n\omega^2_n$, of the PI are obtained as functions of the desired damping ratio, $\zeta$, and undamped natural frequency, $\omega_n$, of the closed-loop second order system ($s^2 + 2\zeta\omega_n + \omega^2_n$) (Ogata, 2002).

### 3.3.3 Asynchronous proportional integral (P+resonant) controller of the output AC voltage

The dynamic equations of the output AC voltage (36), in αβ coordinates, do not present cross coupling terms. Therefore a proportional integral controller, with $\omega_0$ frequency shift, can be used to generate the current references of the DVR (Zmood et al., 2001),

$$H_{PI}(s) = K_P + \frac{K_I\omega_{cut}s}{s^2 + 2\omega_{cut}s + \omega_0^2}. \tag{40}$$

These asynchronous PI controllers, called P+resonant (Li et al., 2007), (Zmood et al., 2001), are tuned to the fundamental frequency $\omega_0$ ($2\pi 50$ rad/s). The practical controller (40) is obtained by approximating the ideal $\omega_0$ integrator using a high-gain low-pass filter with cut-off frequency $\omega_{cut}$ (Zmood et al., 2001). An analysis of the P+resonant controller, applied to DVRs, can be found in (Li et al., 2007).

### 3.3.4 Optimal predictive multilevel DVR current control system

The global performance of the DVR depends significantly on its feedback system, which can be improved using an optimal synchronizer to the fundamental frequency and an optimal predictive controller to track the needed $i_{d\mathrm{Ref}}$ and $i_{q\mathrm{Ref}}$ current references.

The NPC multilevel converter generates the AC currents $i_1$, $i_2$, and $i_3$, tracking references (from $i_{d\mathrm{Ref}}$ and $i_{q\mathrm{Ref}}$) obtained from the output AC voltage controllers (sections 3.3.1 to 3.3.3). These currents are needed to enforce the output AC voltages, and must present low ripple and zero tracking error, to ensure high quality voltage waveforms.

Applying the Kirchhoff laws to the converter circuit (Fig. 16), and the Clarke-Concordia transformation, the dynamic equations of the NPC converter AC output currents, $i_1$, $i_2$, and $i_3$, and the capacitor voltages, $U_{C1}$ and $U_{C2}$, are advantageously represented in αβ coordinates, $i_\alpha$ and $i_\beta$ (41).

$$\begin{bmatrix} \frac{di_\alpha}{dt} \\ \frac{di_\beta}{dt} \\ \frac{dU_{C1}}{dt} \\ \frac{dU_{C2}}{dt} \end{bmatrix} = \begin{bmatrix} -\frac{R}{L} & 0 & \frac{\Gamma_{1\alpha}}{L} & \frac{\Gamma_{2\alpha}}{L} \\ 0 & -\frac{R}{L} & \frac{\Gamma_{1\beta}}{L} & \frac{\Gamma_{2\beta}}{L} \\ -\frac{\Gamma_{1\alpha}}{C_1} & -\frac{\Gamma_{1\beta}}{C_1} & 0 & 0 \\ -\frac{\Gamma_{2\alpha}}{C_2} & -\frac{\Gamma_{2\beta}}{C_2} & 0 & 0 \end{bmatrix} \begin{bmatrix} i_\alpha \\ i_\beta \\ U_{C1} \\ U_{C2} \end{bmatrix} + \begin{bmatrix} -\frac{1}{L} & 0 & 0 \\ 0 & -\frac{1}{L} & 0 \\ 0 & 0 & \frac{1}{C_1} \\ 0 & 0 & \frac{1}{C_2} \end{bmatrix} \begin{bmatrix} \frac{U_{L\alpha} - U_\alpha}{n} \\ \frac{U_{L\beta} - U_\beta}{n} \\ i_{dc} \end{bmatrix} \quad (41)$$

Several control methods for the currents, $i_\alpha$ and $i_\beta$, were proposed (Barros & Silva, 2008), (Kazmierkowski & Malesani, 1998), and (Nabae & Takahashi, 1981). However, the optimal predictive control method (Barros & Silva, 2008) is advantageous, as it both minimizes AC current, $i_\alpha$ and $i_\beta$, errors, and the DC unbalance of capacitor voltages, $U_{C1}$ and $U_{C2}$. Results show comparably better performances in the current waveforms (lower ripple and THD) and on the balancing of capacitor DC voltages. The optimal predictive current controller has the potential to improve the overall performance of the DVR (Barros & Silva, 2010).
The current optimum controller minimizes both the AC currents errors and the capacitor voltage difference using the quadratic cost functional (14) of the tracking errors (15).

### 3.3.5 Simulation and experimental results

Experimental results of the AC voltages at the sensitive loads, $U_{L1}$, $U_{L2}$, and $U_{L3}$, in steady state operation (Fig. 17) show that predictive, PI controllers and P+ressonant controllers ensure tracking of their references showing a nearly perfect sinusoidal waveform.

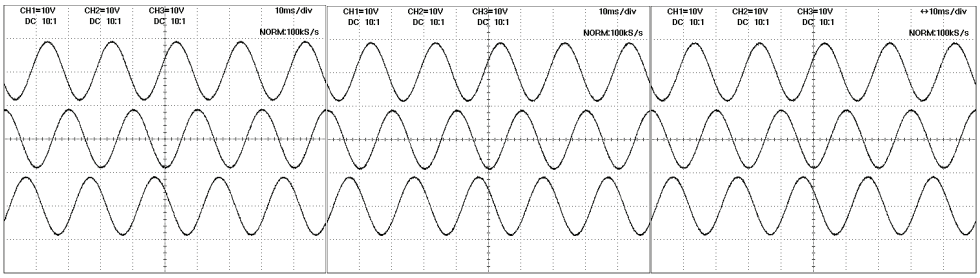


a) Predictive controller. b) Classical PI controller. c) P+resonant controller

Fig. 17. The sensitive load AC voltage at sensitive loads, $U_{L1}$ + 740 V, $U_{L2}$, and $U_{L3}$ - 740 V, in steady state operation (vertical: 370 V/Div and horizontal: 10 ms/Div)

To analyse the influence of load disturbances on the output AC voltage, the load resistive component was altered from the nominal values, $R_L$, to unbalanced values of $R_L/2$, $R_L$, and $2R_L$, respectively in phases 1, 2, and 3, (changes occur at the fifth horizontal division of Fig. 18). The results show (Fig. 18a) that using the optimal predictive output AC voltage controller the sensitive load voltages track their references, being almost insensitive to the unbalanced load step variation. The AC voltage PI controller (Fig. 18b) is not able to control the individual voltage amplitude of the three phases supplying unbalanced loads. The output

AC voltages controlled via the P+resonant (Fig. 18c) are balanced, but present a slowly recovering distortion.

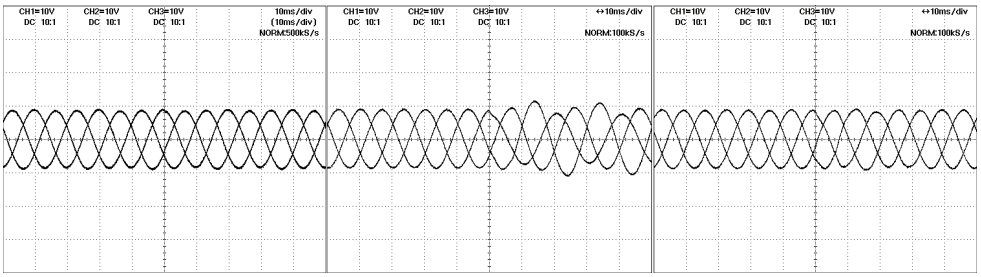

a) Predictive controller. b) Classical PI controller. c) P+resonant controller

Fig. 18. The sensitive load AC voltage, $U_{L1}$, $U_{L2}$, and $U_{L3}$, when is connected an unbalanced load (vertical: 370 V/Div and horizontal: 10 ms/Div)

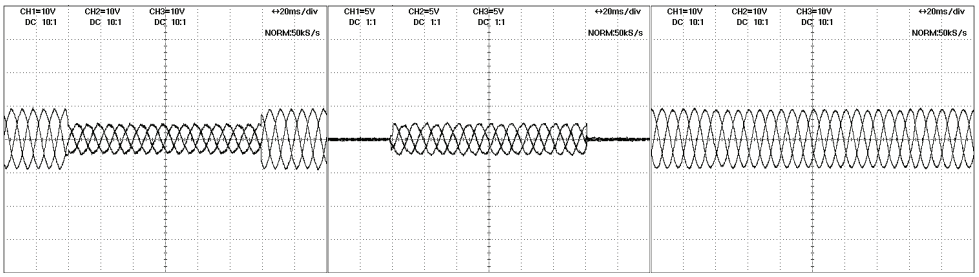

a) AC voltage b) Injected voltages c) Output AC voltage

Fig. 19. Experimental results of the AC voltage sag, $U_1$, $U_2$, and $U_3$, the injected voltages of the DVR, $U_{L1}$-$U_1$, $U_{L2}$-$U_2$, and $U_{L3}$-$U_3$, and the load AC voltage at the sensitive load, $U_{L1}$, $U_{L2}$, and $U_{L3}$, using the optimal predictive controller (370V/Div and 20 ms/Div).

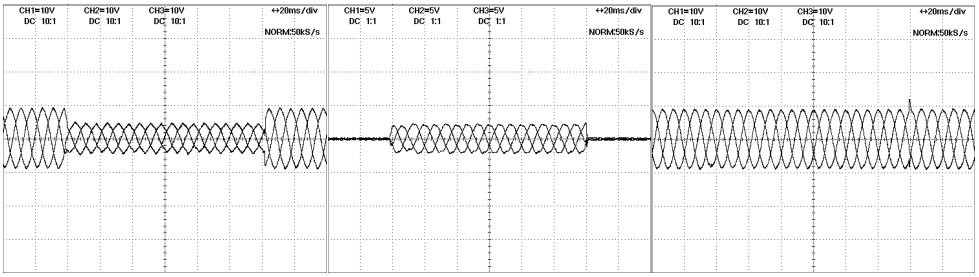

a) AC voltage b) Injected voltages c) Output AC voltage

Fig. 20. Experimental results of the AC voltage sag, $U_1$, $U_2$, and $U_3$, the injected voltages of the DVR, $U_{L1}$-$U_1$, $U_{L2}$-$U_2$, and $U_{L3}$-$U_3$, and the load AC voltage at the sensitive load, $U_{L1}$, $U_{L2}$, and $U_{L3}$, with the filtering capacitor on the NPC converter-side (370V/Div and 20 ms/Div).

During a sag occurrence, (Fig. 19a), reducing to 50% the AC voltages during 120 ms, the NPC converter injects voltages, (Fig. 19b), to mitigate the sag, whose references are calculated using the output AC voltage optimal predictive controller, showing a near perfect critical load voltage waveform.
The NPC converter with the filtering capacitor on the NPC converter-side causes sensitive load transient notches or overshoots at beginning or at the end of the sag, respectively (Fig. 20). Oppositely, the line-side capacitor filtering topology enables sensitive load voltages with constant amplitude and no notches or overshoots (Fig. 19c). As expected this topology improves the power quality and protects sensitive loads from network AC voltage sags, without notches or overshoots. Results obtained when using the PI and the P+resonant controllers show lower performances.

## 4. Conclusion

This chapter presented an optimized control method to the multilevel NPC converter for applications in electrical power quality. The experimental results confirmed these improvements through three applications: filtering the currents of non-linear loads, with an APF, unity power factor AC/DC conversion, with a multilevel UPFR, and mitigation of sags, over-voltages, short interruptions, harmonic distortion, and unbalances in the AC electrical power network with a multilevel DVR.
The proposed optimal predictive controller predicts in real time the state space voltages and currents of the multilevel converter and computes a quadratic cost functional to choose the optimal vector.
Obtained simulation and experimental results show that the NPC converter AC side currents track their references showing comparatively smaller ripple, total harmonic distortion less than 1%, and almost no steady state error (0.3%). The capacitor voltages are balanced with an error lower than 1%, and the balancing are assured even when NPC redundant vectors are not chosen. Near perfect capacitor DC voltage balancing is obtained while reducing current ripples, harmonic distortion and switching frequency.
In the first application to improve power quality, the NPC multilevel converter was connected as APF in parallel to non-linear loads to reduce the injection of harmonic components in the electrical power network, working as APF filter and reactive power compensator so that the power factor was nearly one.
Results confirm that the predictive optimal control of the NPC multilevel converter operating as APF can regulate the DC voltage and reduce the THD of AC line current from 36% to 1% with near-unity power factor (0.997), significantly improving power quality of line voltages.
In section 3.2, the synthesis of UPFR optimum controllers was presented.
The optimal predictive controller of the multilevel converter was used to control the AC currents and to balance the DC capacitors voltage. Comparisons were done to other controllers such as sliding mode, aiming to study the influence of state space control methods in the multilevel converter performance in applications to improve the electrical power quality.
Results show that the multilevel UPFR DC voltage follows the reference value without steady error and the input AC currents are sinusoidal in phase with the AC voltages. The

optimal predictive controller reduces the AC current ripple factor from 9% to 1%, and reduces THD of the AC current from 8% to 1%, compared to the sliding mode controller.
The optimized multilevel DVR here proposed vastly improves power quality at sensitive critical loads. The performance of the optimal predictive controller generating the reference voltages to inject was compared to the synchronous dq frame PI controller and to the P+resonant controller. Results show that predictive controllers present the lowest THD levels in the load AC voltages, are able to regulate unbalanced loads AC voltages, allow plug-in and out of extra loads without causing swells, sags, notches or overshoots, and reduce the distortion of AC voltages in non-linear loads. Load AC voltages are almost sinusoidal, when facing balanced and unbalanced sags, and short interruptions with unbalanced loads. Voltage THD is reduced to values lower than 1%, the DVR behaving also as a series active power filter for the AC voltages strongly improving the power quality of sensitive loads.

## 5. References


Barros, J. D.; Fekri, S. & Athans, M. (2005). Robust mixed-mu synthesis performance for mass-spring system with stiffness uncertainty, *Proceedings of IEEE 13th Mediterranean Conference on Control and Automation MED05*, pp. 743-748, ISBN: 0-7803-8936-0, Cyprus, June 2005, IEEE, Limassol

Barros, J. D. & Silva, J. F. (2008). Optimal predictive control of three-phase NPC multilevel converter for power quality applications. *IEEE Transactions on Industrial Electronics,* Vol. 55, No. 10, (October 2008) pp. 3670-3681, ISSN: 0278-0046

Barros, J. D. & Silva, J. F. (2010). Multilevel optimal predictive dynamic voltage restorer. *IEEE Transactions on Industrial Electronics,* Vol. 57, No. 8, (August 2010) pp. 2747-2760, ISSN: 0278-0046

Holmes, D. G. & Lipo, T. A. (2003). *Pulse Width Modulation for Power Converters,* Wiley-Interscience, John Wiley & Sons, Canada

Jones, C. V. (1967). *The Unified Theory of Electrical Machines,* Plenum, New York

Kazmierkowski, M. P. & Malesani, L. (1998). Current control techniques for three-phase voltage-source PWM converters: a survey. *IEEE Trans. Ind. Electron.,* Vol. 45, No. 5, (October 1998) pp. 691-703, ISSN: 0278-0046

Kwakernaak, H. & Sivan, R. (1972). *Linear Optimal Control Systems,* Wiley-Interscience, John Wiley & Sons, ISBN: 0-471-51110-2, Canada

Li, Y. W.; Blaabjerg, F.; Vilathgamuwa, D. M. & Loh, P. C. (2007). Design and comparison of high performance stationary-frame controllers for DVR implementation. *IEEE Trans. Power Electron.,* Vol. 22, (March 2007) pp. 602-612, ISSN: 0885-8993

Marchesoni, M.; Mazzucchelli, M. & Tenconi, S. (1988). A non conventional power converter for plasma stabilization, *Proceedings of Power Electronics Specialists Conference PESC88*, pp. 122-129, Japan, April 1988, IEEE, Kyoto

Meynard, A. & Foch, H. (1992). Multi-level choppers for high voltage applications. *EPE Journal,* Vol. 2, (March 1992) pp. 45-50

Moreno-Muñoz, A. (2007). *Power Quality: Mitigation Technologies in a Distributed Environment,* Springer, ISBN: 1612-1287, London

Nabae, A. & Takahashi, I. (1981). A new neutral-point-clamped PWM inverter. *IEEE Trans. Ind. Applicat.,* Vol. IA-17, (Sep./Oct. 1981) pp. 518-523, ISSN: 0093-9994

Ogata, K. (2002). *Modern Control Engineering,* Prentice Hall, 4th edition, USA

Silva, J. (1999). Sliding-mode control of boost-type unity-power-factor PWM rectifiers. *IEEE Trans. on Ind. Electron.,* Vol. 46, No. 3, (June 1999) pp. 594-603, ISSN: 0278-0046

Singh ,B.; Al-Haddad, K. & Chandra, A. (1999). A review of active filters for power quality improvement. *IEEE Transactions on Industrial Electronics,* Vol. 46, No. 5, (October 1999) pp. 960-971, ISSN: 0278-0046

Tan, T. L.; Chen, S. & Choi, S. S. (2005). An overview of power quality state estimation, Proceedings of the 7th International Power Engineering Conference IPEC 2005, pp. 1-5, ISBN: 981-05-5702-7, Singapore, November/December 2005, IEEE

Zmood, D. N.; Holmes, D. G. & Bode, G. H. (2001). Frequency-domain analysis of three-phase linear current regulators. *IEEE Trans. Ind. Applicat.,* Vol. 37, No. 2, (March/April 2001) pp. 601-610, ISSN: 0093-9994

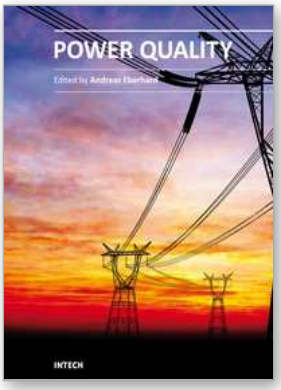


**Power Quality**

Edited by Mr Andreas Eberhard

ISBN 978-953-307-180-0
Hard cover, 362 pages
**Publisher** InTech
**Published online** 11, April, 2011
**Published in print edition** April, 2011

Almost all experts are in agreement - although we will see an improvement in metering and control of the power flow, Power Quality will suffer. This book will give an overview of how power quality might impact our lives today and tomorrow, introduce new ways to monitor power quality and inform us about interesting possibilities to mitigate power quality problems.

**How to reference**

In order to correctly reference this scholarly work, feel free to copy and paste the following:

João Dionísio Simões Barros and José Fernando Alves da Silva (2011). Power Quality Enhancement using Predictive Controlled Multilevel Converters, Power Quality, Mr Andreas Eberhard (Ed.), ISBN: 978-953-307-180-0, InTech, Available from: http://www.intechopen.com/books/power-quality/power-quality-enhancement-using-predictive-controlled-multilevel-converters

INTECH
open science | open minds

**InTech Europe**
University Campus STeP Ri
Slavka Krautzeka 83/A
51000 Rijeka, Croatia
Phone: +385 (51) 770 447
Fax: +385 (51) 686 166
www.intechopen.com

**InTech China**
Unit 405, Office Block, Hotel Equatorial Shanghai
No.65, Yan An Road (West), Shanghai, 200040, China
中国上海市延安西路65号上海国际贵都大饭店办公楼405单元
Phone: +86-21-62489820
Fax: +86-21-62489821